Recent changes in Arctic sea ice melt onset, freezeup, and melt season length

Thorsten Markus,[1] Julienne C. Stroeve,[2] and Jeffrey Miller[3]

Received 13 April 2009; revised 18 August 2009; accepted 4 September 2009; published 29 December 2009.

[1] In order to explore changes and trends in the timing of Arctic sea ice melt onset and freezeup, and therefore melt season length, we developed a method that obtains this information directly from satellite passive microwave data, creating a consistent data set from 1979 through present. We furthermore distinguish between early melt (the first day of the year when melt is detected) and the first day of continuous melt. A similar distinction is made for the freezeup. Using this method we analyze trends in melt onset and freezeup for 10 different Arctic regions. In all regions except for the Sea of Okhotsk, which shows a very slight and statistically insignificant positive trend (0.4 d decade^{-1}), trends in melt onset are negative, i.e., toward earlier melt. The trends range from -1.0 d decade^{-1} for the Bering Sea to -7.3 d decade^{-1} for the East Greenland Sea. Except for the Sea of Okhotsk all areas also show a trend toward later autumn freeze onset. The Chukchi/Beaufort seas and Laptev/East Siberian seas observe the strongest trends with 7 d decade^{-1}. For the entire Arctic, the melt season length has increased by about 20 days over the last 30 years. Largest trends of over 10 d decade^{-1} are seen for Hudson Bay, the East Greenland Sea, the Laptev/East Siberian seas, and the Chukchi/Beaufort seas. Those trends are statistically significant at the 99% level.

Citation: Markus, T., J. C. Stroeve, and J. Miller (2009), Recent changes in Arctic sea ice melt onset, freezeup, and melt season length, *J. Geophys. Res.*, *114*, C12024, doi:10.1029/2009JC005436.

1. Introduction

[2] The onset of melt and melt season length are important variables for understanding the Arctic climate system. Given the recent large losses of the Arctic summer sea ice cover [*Stroeve et al.*, 2005, 2008] it has become critical to investigate the causes of the widespread decline in Arctic sea ice and the consequences of its continued decline. Extended or more extensive sea ice melt in response to increasing atmospheric temperatures may be one of the primary drivers of reduced summer sea ice. *Perovich et al.* [2007] found that the total amount of solar energy absorbed during the summer melt season was strongly related to the timing of when melt begins. Earlier melt onset allows for earlier development of open water areas that in turn enhance the ice-albedo feedback. Several approaches exist to determine melt and freeze onset of Arctic sea ice from satellite passive microwave data [e.g., *Smith*, 1998b; *Drobot and Anderson*, 2001; *Belchansky et al.*, 2004]. In addition to passive microwave data, other instruments have been or can be utilized to determine melt conditions of Arctic sea ice. For example, algorithms have been developed to detect melt from active microwave data, e.g., scatterometers [*Drinkwater and Liu*, 2000; *Forster et al.*, 2001], and SAR data [*Winebrenner et al.*, 1994; *Kwok et al.*, 2003]. Melt onset and freezeup of Arctic sea ice has also been determined using buoy data from the International Arctic Buoy Program/Polar Exchange at the Sea Surface IABP/POLES [*Rigor et al.*, 2000].

[3] Advantages of using satellite passive microwave data over buoy data, for example, are (1) its large spatial coverage, (2) its relatively long and consistent record of observations (starting in 1979), and (3) the fact that microwave emission is directly related to the melt signature of sea ice (or the overlying snow cover). The dielectric properties of snow and ice, and therefore their emissivities, change drastically with ice and snow wetness. When meltwater forms at the surface, the emissivity increases to close to 1 causing the surface to appear as a blackbody at microwave wavelengths. Following this initial melt, the snow/ice will either increase in wetness or it will refreeze (most likely during the night), strongly affecting the temporal evolution of the microwave signature. If wetness increases, the snow emissivity eventually approaches the emissivity of open water (even before the development of melt ponds). During refreezing, the polymorphic aggregation of snow grains under equitemperature metamorphosis results in very large snow grains that cause increased scattering and therefore a reduction in brightness temperatures (T_B). The reduction is more pronounced at 37 GHz than at 19 GHz. *Drobot and Anderson* [2001] developed a method (referred to as the

[1]Cryospheric Sciences Branch, NASA Goddard Space Flight Center, Greenbelt, Maryland, USA.
[2]National Snow and Ice Data Center, University of Colorado, Boulder, Colorado, USA.
[3]Wyle Information Sciences, NASA Goddard Space Flight Center, Greenbelt, Maryland, USA.

Copyright 2009 by the American Geophysical Union.
0148-0227/09/2009JC005436

Table 1. Data Periods for the Different Satellite Passive Microwave Radiometers

Satellite/Instrument	Start Date	End Date
Nimbus-7 SMMR	Oct 1978	Aug 1987
F-08 SSM/I	Jul 1987	Dec 1991
F-11 SSM/I	Dec 1991	May 1995
F-13 SSM/I	May 1995	present

advanced horizontal range algorithm (AHRA)) to determine melt onset for the entire Arctic using temporal variations in 19 and 37 GHz T_B but do not determine the freezeup date. *Smith* [1998a] determined the onset of melt and freezeup using a combination of 19 and 37 GHz brightness temperatures, but only for perennial sea ice. *Belchansky et al.* [2004] calculated melt season length using a combination of passive microwave data (similar to the AHRA algorithm) and surface air temperatures from the POLES data set. The addition of the POLES data helped ensure the passive microwave melt onset was within a reasonable range, helping to eliminate erroneous microwave melt signals.

[4] In this paper, we build upon the above mentioned approaches to calculate both melt and freeze onset dates, and therefore melt season length for the entire Arctic using passive microwave data only. This has the advantage of a consistent data set starting back in 1979.

[5] In development of the melt/freeze algorithm, it was important to clearly define the onset of melt and the onset of freezeup. In this paper, we distinguish between the first melt event (early melt onset (EMO)) and continuous melt (melt onset (MO)). EMO is the day of the first occurrence of melt independent of whether temperatures remain above freezing or not. Onset of continuous melt (MO) is defined as the day after which the sea ice stays under melt conditions for the summer. This is very similar to the definition of *Livingstone et al.* [1987] who define "early melt" as a transition period starting transformation of snowpack due to melt-freeze cycles. "Melt onset" is defined when free water is continuously present in the snowpack; and "freezeup" is defined when the average surface temperature is at the melting point and young ice grows in open water areas. Studies have shown that the daily variance in brightness temperature begins to increase in response to "early melt" and increases until it reaches a maximum at the transition from the melt onset period (in this paper "transition period") to advanced melt (in this paper "melt") [*Harouche and Barber*, 2001]. Similarly, we distinguish between the first day freezeup occurs (early freeze onset (EFO)) and the day when freezing conditions persist for the rest of the winter season (freeze onset (FO)).

[6] We compare our results with near-surface air temperature data sets from climate models (NCEP/NCAR reanalysis project [*Kalnay et al.*, 1996]) and from buoys (the International Arctic Buoy Program/Polar Exchange at the Sea Surface (IABP/POLES) [*Rigor et al.*, 2000]), and explore regional trends in melt onset, freezeup, and melt season length.

2. Data

[7] This study uses daily averaged brightness temperatures from SMMR [*Gloersen et al.*, 1990] and SSM/I [*Maslanik and Stroeve*, 1990] mapped to the 25 km polar stereographic grid available at the National Snow and Ice Data Center (NSIDC) in Boulder, Colorado. Different sensors on different satellites provide a continuous time series of multichannel passive microwave brightness temperatures since 1979 (Table 1). Overlap periods between sensors have been used to intercalibrate the different instruments, thereby ensuring a consistent long-term time series. Because previous melt algorithms were developed for SSM/I, we regressed SMMR T_Bs toward SSM/I using the overlap period in 1987. The results are similar to those of *Jezek et al.* [1993], but we used the F-08 SSM/I as the baseline instead of SMMR. For the transition from F-08 to F-11 and from F-11 to F-13 we used the coefficients derived by *Abdalati et al.* [1995] and *Stroeve et al.* [1998], respectively, although studies have shown that intersensor offsets are generally less than 1 K [*Colton and Poe*, 1999]. Since our melt detection involves the use of temporal variability between days, slight offsets in T_Bs between sensors should not affect the results. Because the SSM/I has a wider swath compared to SMMR the gap of missing data around the pole is different. For consistency, averages and trends are calculated using only pixels that have coverage from both, SMMR and SSM/I. In addition, the same land mask is applied to both data sets. The length of the data record used in this paper goes through 2007.

3. Approach

[8] The strategy of this method is to take advantage of several indicators of melt and freeze onset inherent in the data and explore their agreement. The combined approach builds on the strength of multiple indicators, each sensitive to different features of melt. Specifically, we utilize the agreement of different indicators (especially since they have different advantages and limitations) and also make use of the strength of the melt signal. Generally, for dry snow conditions volume scattering is dominant whereas with the onset of melt, volumetric moisture content increases and surface scattering becomes dominant. Since surface scattering is smaller compared to the volume scattering, a sharp increase in emissivity occurs when the snow becomes wet (see, for example, *Ulaby et al.* [1986]).

[9] The algorithm, referred to here as the PMW algorithm, is described with the help of two examples that contain to the two principal Arctic sea ice types: perennial (multiyear) sea ice (Figure 1) and seasonal (first-year) sea ice (Figure 2).

[10] The three primary indicators used are given in equations (1)–(3).

$$\Delta 37 = |T_B(37V)(i+1) - T_B(37V)(i)|. \quad (1)$$

[11] The absolute difference in $T_B(37V)$, $\Delta 37$, between day i and day i + 1 takes advantage of differences in temporal variability between freezing and melting conditions (see Figures 1b and 2b). For most of the winter time (until about days 140–150 in Figures 1a and 1b) the brightness temperatures show little temporal variation (generally between 5 to 10 K). This changes noticeably when melt begins. $\Delta 37$ shows a significant increase in variability (up to 25 to 30 K)

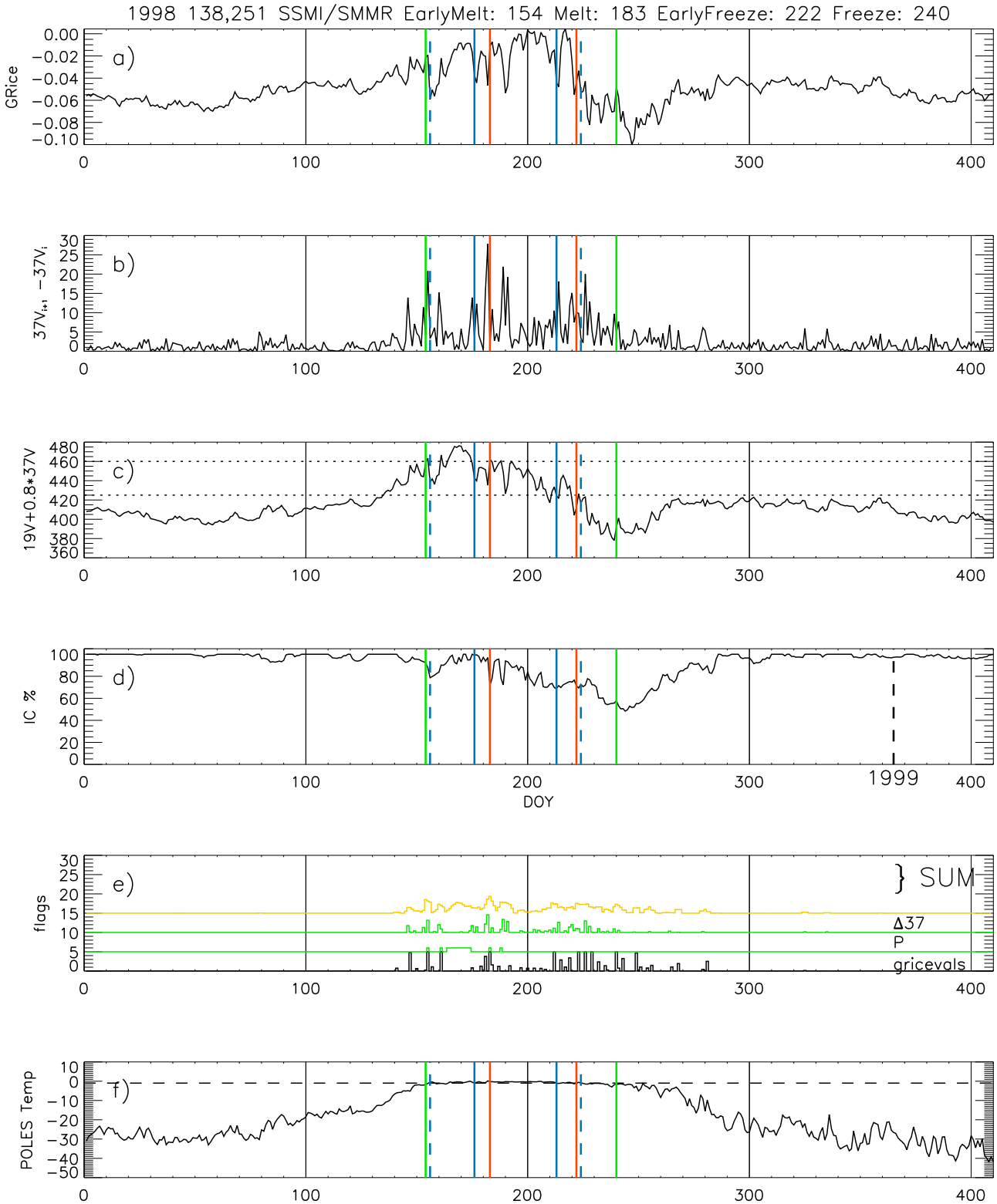

Figure 1. Example of method for a pixel in the central Arctic (80.6°N, 157.5°E). (a) Spectral gradient ratio of T_B(19V) and T_B(37V) corrected for ice concentration, (b) daily change in T_B(37V), (c) P-value as defined by *Smith* [1998a], (d) NASA Team ice concentration, (e) summary of criteria (see text for details), and (f) POLES temperature; the vertical red line indicates the passive microwave derived melt and freeze onset; the green lines indicate early and permanent freeze; the solid and dotted blue lines indicate the periods of continuous summer melt (days between the solid lines) and maximum melt (days between the dotted lines) derived from the POLES data.

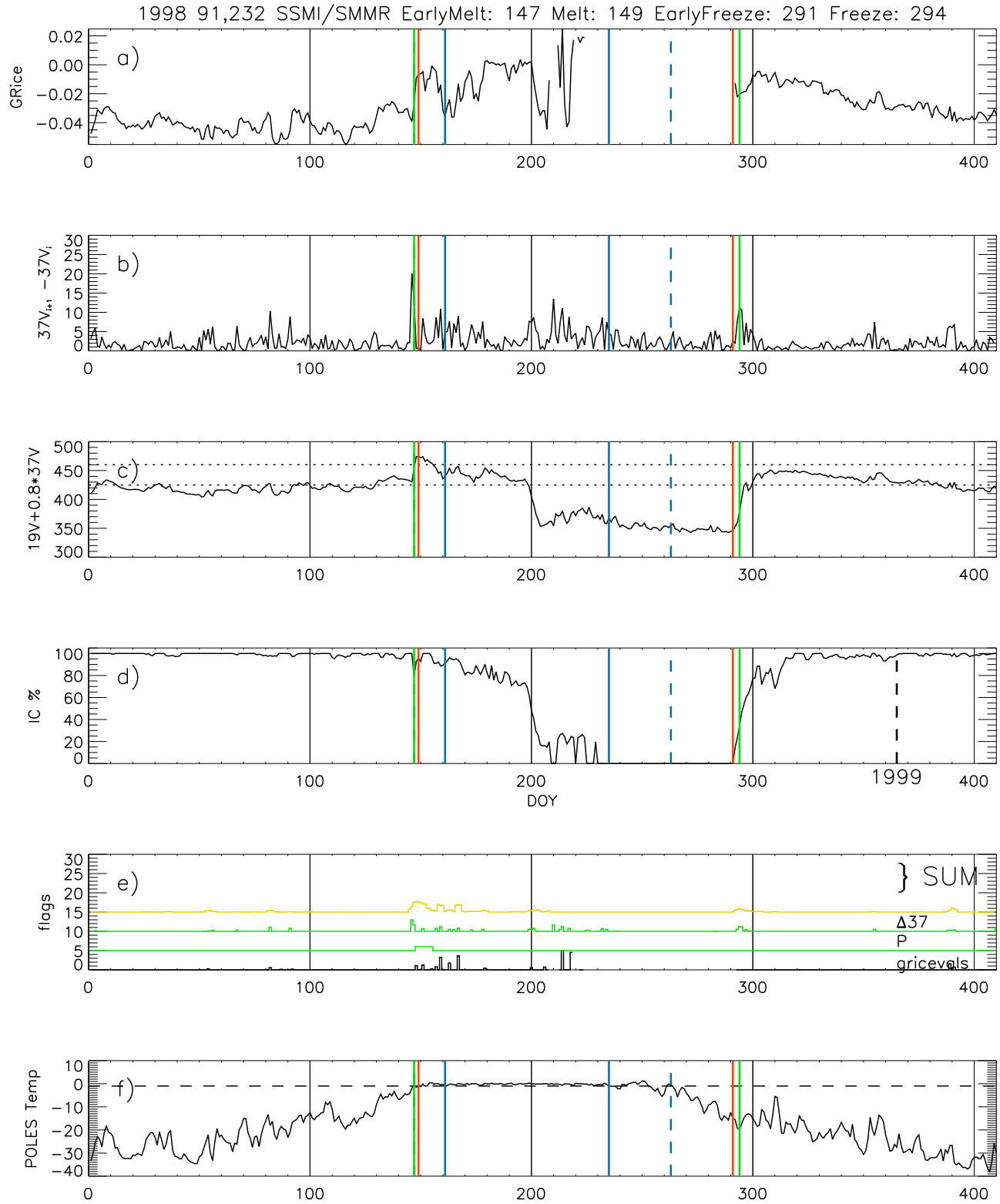

Figure 2. Same a Figure 1 but for the Bering Sea (75.6°N, 136.4°W). The first blue dashed line (first melt in the POLES data) is invisible because it coincides with the PMW early melt (green line).

when melt conditions are present and is a similar melt onset indicator as what is used in the AHRA algorithm.

$$\Delta\ GR_{ice} = GR_{ice}(i) - GR_{ice}(i+1) \quad (2)$$

[12] This parameter also utilizes temporal variability and is used because it explicitly accounts for the effects of variations in sea ice concentration. Brightness temperatures, T_{Bice}, are calculated to reflect only the ice-covered portion of the measured brightness temperature, i.e.,

$T_{Bice} = (T_B - (1 - C)T_{Bow})/C$, where T_B is the measured brightness temperature, C the sea ice concentration, and T_{Bow} a constant brightness temperature for the open ocean [see also *Markus and Cavalieri*, 1998]. $GR_{ice}(i)$ is the spectral gradient ratio for day i defined as

$$GR_{ice} = (T_{Bice}(37V) - T_{Bice}(19V))/(T_{Bice}(37V) + T_{Bice}(19V)).$$

[13] During winter GR_{ice} is negative for multiyear ice (Figure 1a, $GR_{ice} \simeq -0.06$) and slightly negative for first-year ice (Figure 2a, $GR_{ice} \simeq -0.01$). During the melt-freeze transition periods, GR_{ice} varies between values of zero for a slightly wet snow cover and more negative values when the snow refreezes. The same signature is seen for first-year and multiyear ice.

$$P = T_B(19V) + 0.8T_B(37V) \quad (3)$$

[14] Following *Smith* [1998a], this value is used as a discrete threshold for melt and freeze (Figures 1c and 2c). For dry multiyear ice P has values less than 460 K and increases above this value at the onset of melt [*Smith*, 1998a]. For first-year ice, P is greater than 440 for dry snow conditions and drops below that value at the onset of melt. First-year ice pixels are identified when $P > 400$ and $GR_{ice} > -0.03$ on 1 April. The accurate identification of multiyear ice is of minor importance since it is only needed to discern whether an increase or decrease in P is expected as a result of melt. No distinction between first-year ice and multiyear ice is necessary for $\Delta 37$ and ΔGR_{ice}.

[15] For each of the above three parameters, we calculate the strength of the melt (or freeze) signal by normalizing the expected ranges and using them as weights for melt and freeze onset determination. For example, ΔGR range between 0.005 and 0.015 when melt is potentially present. A value of ΔGR of 0.005 is slightly above the noise level whereas a value of 0.015 is a significant jump and consequently a strong indicator of melt. We, therefore, normalize ΔGR values between 0.005 and 0.015 to form a "melt signature weight" ($W_{\Delta GR}$). Similar steps are taken for $\Delta 37$ for which the range is between 5 and 30 K, and P for which the range is between 460 and 490 K for multiyear ice and between 420 and 440 K for FY ice. For each day, the sum of those weights is calculated

$$W = W\Delta_{GR} + W\Delta_{37} + W_P.$$

[16] The day with the greatest sum is the first choice for the melt onset day. The weights and their sum (multiplied by 5) are shown in Figures 1e and 2e. The greatest weights indicate the beginning and ending of the period of continuous melt (referred to as melt onset (MO) and early freeze onset (EFO) and are shown as red lines in Figures 1f and 2f). The first day of melt (EMO) and the very last day of melt (FO) are identified by secondary peaks in W before and after the melt start and end days (green lines in Figures 1f and 2f). It is possible that no early melt signal is detected. A reason could be, for example, the occurrence of EMO and MO on the same day. In this case no EMO is archived.

[17] Noisy results can be an artifact when using temporal information. In order to exclude the effects of spurious brightness temperatures variations, for each pixel W is also calculated for the eight adjacent pixels. For the melt and freeze onsets we can reasonably assume mesoscale coherency. Therefore, if more than four of the surrounding pixels do not differ by more than one day in melt or freeze onset date the value for this pixel is assumed valid. As an estimate of quality or confidence, the total sum of the nine weights is archived. A similar procedure is employed for the freeze onset.

[18] For areas of relatively thin ice, especially near the marginal sea ice zones, we additionally need to include sea ice concentration information since melt onset and the disintegration of the sea ice occur at about the same time (Figures 1d and 2d). Therefore, if no clear melt signal is detected, the day when the ice concentration drops below 80% for the last time before the area becomes sea ice free for the summer is used as the melt onset date. This 80% threshold is somewhat arbitrary but the complete disintegration of sea ice typically occurs rather rapidly. Similarly for the freezeup, when open water is present during summer, the first date at which the ice concentration is above 80% is used as the freeze onset date. Pixels with less than 5 days of ice concentrations above 80% for the entire year are marked as being ice-free.

[19] Figures 1f and 2f show the POLES surface temperature data for the same two locations discussed above. Similar to the PMW algorithm, we distinguish between the first day of temperatures above freezing (first blue dashed line), the day after which the temperature remains above freezing for the rest of the summer (first solid blue line), the first day the temperature drops below freezing (second solid blue line) and the last day for which the temperature is above freezing (second dashed blue line). Therefore, the time between the solid lines represents the minimum melt season length and the time between the dashed lines the maximum melt season length according to the POLES data.

[20] For multiyear ice (Figure 1) PMW and POLES data agree on the first day of melt (EMO). The beginning of continuous melt (MO) is identified 8 days later in the PMW compared to the POLES data. For the freezeup the early freeze (EFO) in PMW agrees with the POLES last day of temperatures above freezing, which is 14 days later in the PMW results. It should be noted, though, that the POLES temperatures are rather constant during the summer months so that small changes in the POLES threshold for determining melt conditions may significantly change the agreement between the two methods. The PMW results are within the error margin of the POLES results. Varying the threshold applied to POLES temperature by +/−2°C resulted in a range of +/−50 days for melt and +/−20 to +/−30 days for freeze. For first-year ice (Figure 2) PMW detects EMO and MO at almost the same time, which, in this case, agrees with the first day of melt in the POLES data. The PMW freezeup is considerably later than the POLES data. The reason for this is that the PMW ice freezeup date for seasonal ice corresponds to the date when ice first reappears at 80% ice concentration.

[21] To illustrate the performance on a larger scale, Figure 3 shows melt onset and freezeup dates in 2004 for

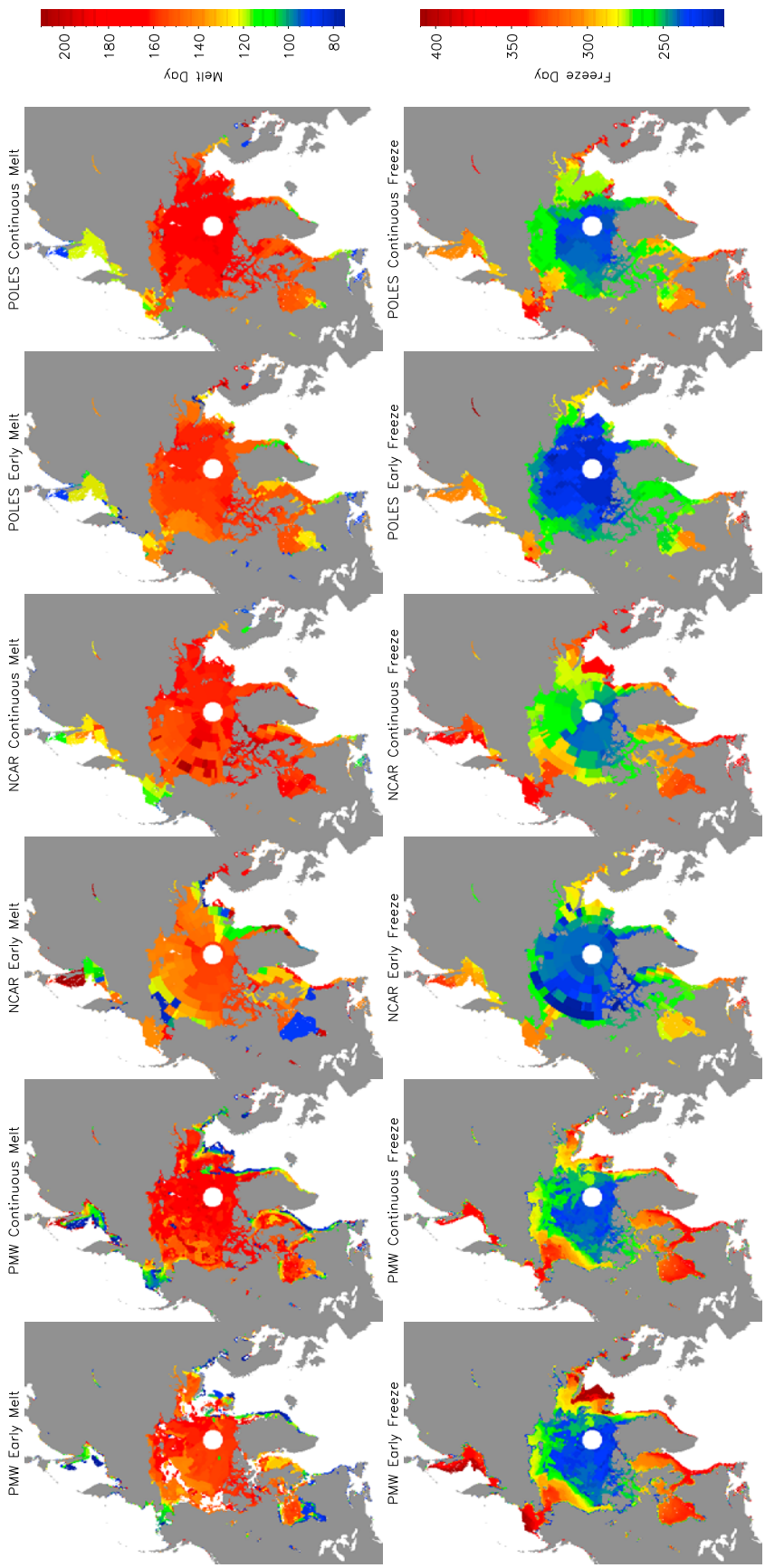

Figure 3. Examples of melt onset and freezeup for 2004 from passive microwave data and from the NCEP/NCAR and POLES data sets. NCAR and POLES melt and freeze onset data are determined by a threshold in temperature of −1°C. Temperatures above this threshold indicate melt conditions. For the POLES data we distinguish between earliest melt and continuous melt, as well as earliest freeze and continuous freeze. "Earliest melt" indicates the day when temperatures go above the threshold temperature for the first time while "continuous melt" indicates the day when temperatures remain above the threshold temperature for the summer. Corresponding criteria are applied for "earliest freeze" and "continuous freeze."

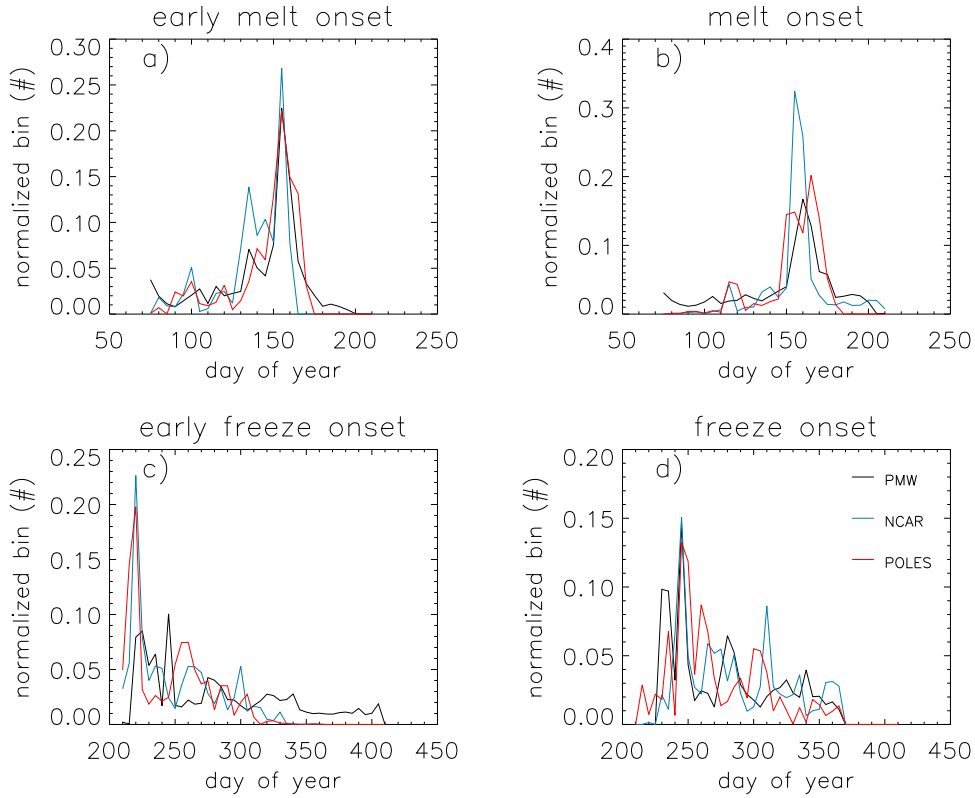

Figure 4. Distributions of early melt onset, melt onset, early freeze onset, and freeze onset for the PMW, POLES, and NCEP/NCAR data for the year 2004.

the entire Arctic juxtaposed to the melt onset and freezeup dates derived from the NCEP/NCAR and POLES near-surface air temperature data sets. A threshold of $-1°C$ is applied to both temperature data sets. For melt, there is very good agreement between the PMW and POLES results for both EMO and MO. Except for the Bering Sea and the Sea of Okhotsk, spatial patterns as well as actual melt onset days are in good agreement. On a large scale, there is not much difference between the EFO and FO days in the PMW data set (at least in 2004). Freezeup days for seasonal sea ice are very different between the PMW and the NCEP/NCAR and POLES data sets. This is expected, though, because of the time it takes to cool the water down to freezing after the air temperatures have dropped below 0°C. For the central Arctic, PMW freezeup dates agree best with the POLES continuous freeze days. In Figure 4 the distributions EMO, MO, EFO, and FO are compared. In general the shape of the distributions for the different quantities is in very good agreement between the different data sets. For EMO and MO, areal increase in melt onset slowly increases until a strong peak is reached, with little melt after that peak. The agreement on the date of the main peak is excellent for

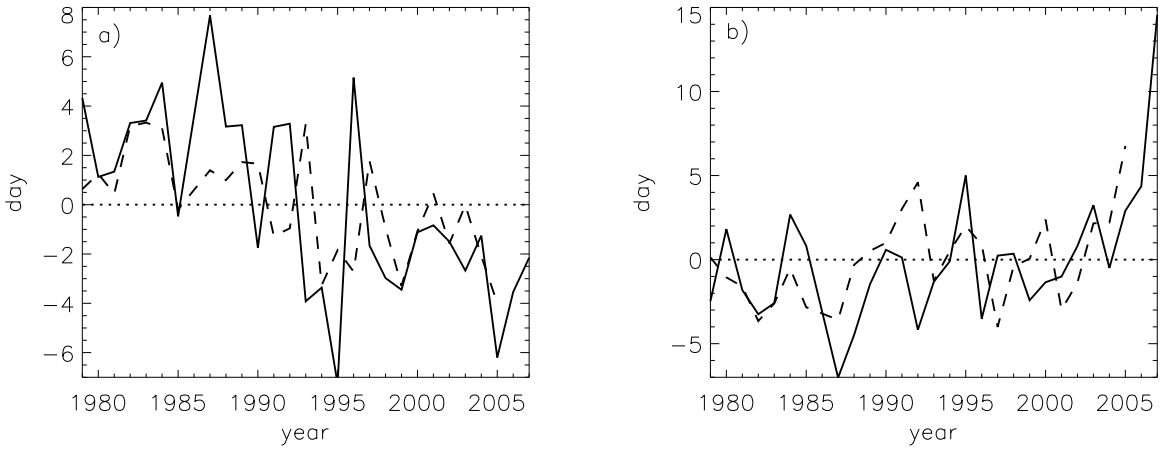

Figure 5. Anomalies of (a) melt onset and (b) freezeup from the PMW data (solid lines) and POLES data (dashed lines) for the entire Arctic.

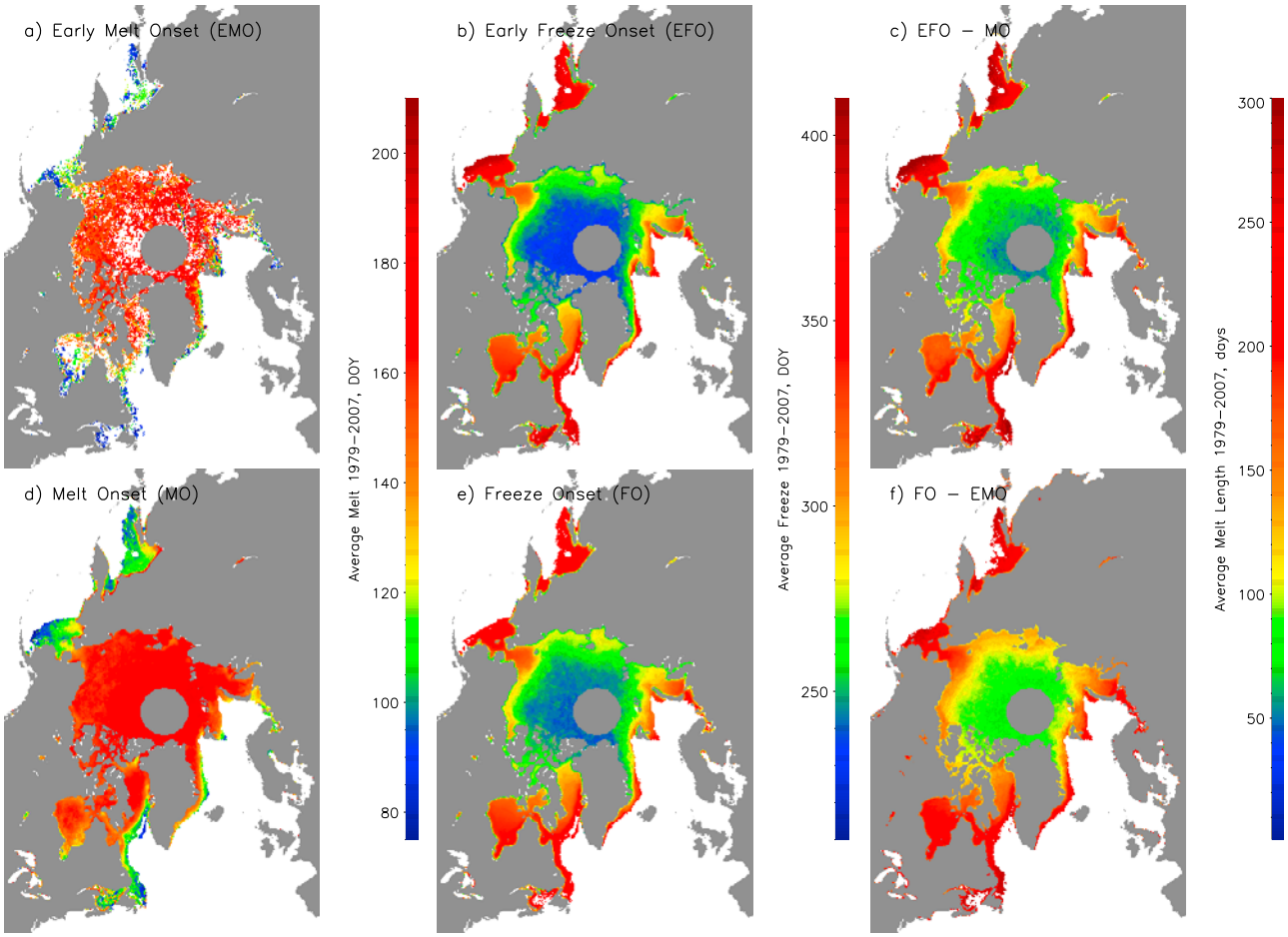

Figure 6. Average (a) early melt onset (EMO) day, (d) melt onset (MO) day, (b) early freezeup (EFO) day, (e) freezeup (FO) day as well as (c) "inner" melt length (EFO−MO) and (f) "outer" melt length (FO−EMO) for the period of 1979−2005. The reason for the color scale going up to day 400 is that in the seasonal sea ice zone the onset of freeze does often commence not before January or February the following year.

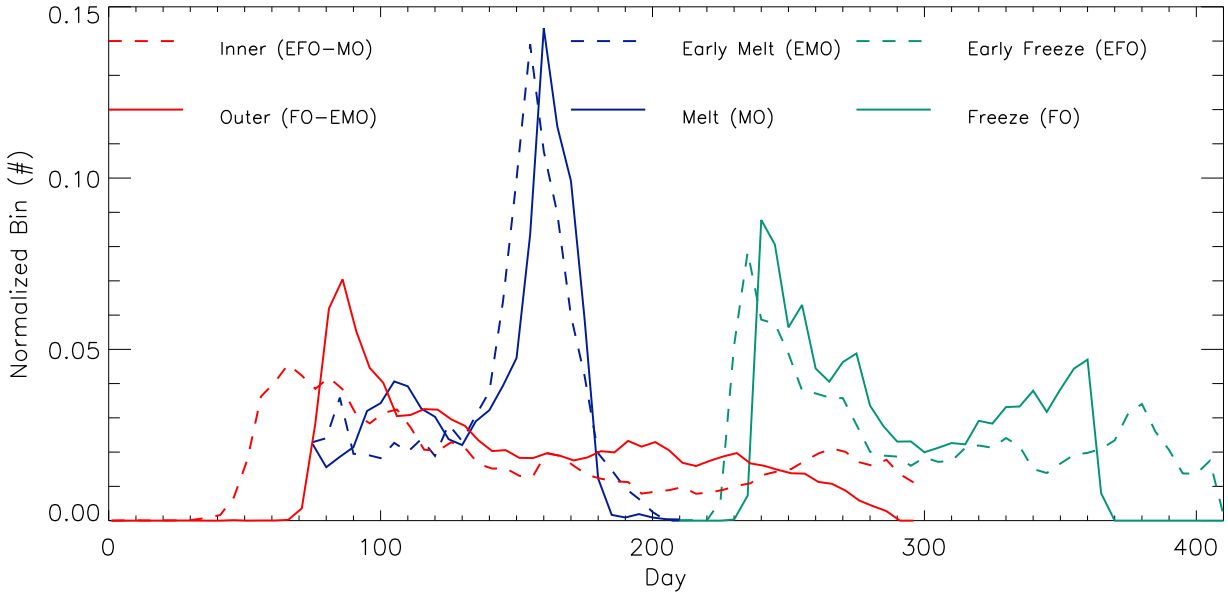

Figure 7. Distributions of average melt onset (EMO and MO), freeze onset (EFO and FO), and melt season length derived from the PMW data set.

Table 2. Average Melt and Freeze Onset Days as Well as Melt Season Length for Different Regions[a]

Region	Early Melt (EMO)	Melt (MO)	Early Freeze (EFO)	Freeze (FO)	"Inner" Melt Length (EFO−MO)	"Outer" Melt Length (FO−EMO)
All	144.1 (3.6)	160.4 (3.7)	272.8 (4.5)	281.5 (4.0)	112.4 (7.5)	137.5 (6.6)
Sea of Okhotsk (1)	110.0 (6.3)	131.3 (7.4)	311.2 (8.2)	323.4 (7.7)	179.8 (11.9)	213.3 (10.4)
Bering Sea (2)	104.5 (7.5)	123.9 (7.4)	312.0 (10.9)	324.1 (9.9)	188.1 (14.5)	219.6 (13.9)
Hudson Bay (3)	126.4 (8.2)	151.1 (8.1)	313.9 (8.5)	321.6 (7.1)	162.8 (15.1)	195.2 (14.1)
Baffin Bay (4)	136.7 (8.2)	155.0 (7.3)	302.4 (7.3)	310.3 (6.5)	147.4 (12.2)	173.6 (12.0)
East Greenland (5)	137.1 (9.9)	153.2 (9.2)	269.2 (10.1)	282.4 (11.2)	116.0 (16.3)	145.3 (16.9)
Kara/Barents Seas (6)	142.9 (8.1)	160.1 (6.6)	281.6 (7.8)	291.0 (8.0)	121.5 (11.7)	148.1 (12.1)
Central Arctic (7)	161.1 (5.4)	175.2 (5.0)	239.4 (5.1)	248.8 (5.5)	64.2 (7.6)	87.7 (7.4)
Canadian Archipelago (8)	152.2 (5.7)	161.2 (4.9)	252.5 (5.8)	261.7 (6.0)	91.4 (8.9)	109.6 (9.7)
Laptev/East Siberian seas (9)	153.7 (5.8)	166.9 (4.9)	257.7 (11.1)	264.9 (10.2)	90.9 (14.4)	111.2 (14.2)
Chukchi/Beaufort seas (10)	148.4 (6.1)	162.2 (4.8)	261.6 (11.3)	269.7 (10.2)	99.4 (14.6)	121.3 (13.9)

[a]The numbers in parentheses are the standard deviations. See also Figure 8 for illustration of regions.

EMO, and for MO the PMW peak lies between the POLES and NCEP/NCAR peaks. For EFO and FO the distribution is broader with a peak toward the beginning of the freezeup period. A notable difference between the data sets can be seen for EFO where the PMW data show a longer tail, which is a result of the time difference between when the air temperature reaches freezing and when the water temperature reaches freezing. Areas with later EFOs in the PMW data are generally the Bering Sea and the Sea of Okhotsk. Over a longer time span (Figure 5) annual anomalies in melt onset and freezeup derived from the PMW and POLES data do not always line up but the magnitude and the overall trend agree well.

4. Averages and Trends

[22] Average melt and freezeup maps show, as expected, a strong latitudinal dependence (Figure 6), with earlier melt starting in the marginal seas and spreading northward as the summer progresses. Similarly, earliest freezeup occurs in the central Arctic and expands southward. The distributions are shown in Figure 7. The shapes of the melt and freeze onset distributions are generally similar to the distributions shown in Figure 4. The late EFO dates (with no corresponding FO dates) are a result of seasonal sea ice for which no FO signal could be detected. Table 2 summarizes the average date of melt onset and freezeup, as well as the total number of days of the melt season (i.e., melt season length) for several Arctic regions (see Figure 8) from 1979 through 2007. On average, basin-wide EMO occurs on day 144 (Table 2), which spreads from day 105 for the Bering Sea to day 161 for the central Arctic. MO is on average 16 days later. The central Arctic has the earliest freezeup (day 239) and the Sea of Okhotsk the latest. Melt length varies between 64 and 188 days for the period between continuous melt and early freezeup (EFO−MO), and between 88 and 220 days for the period between first melt and permanent freeze (EMO−FO). The transition period during freezeup is generally shorter than the melt transition period. The melt and freeze days for the Archipelago are in excellent agreement with a recent study using QuikSCAT data that found an average melt day of 150 and an average freezeup day of 266 for the period 2000−2007 [*Howell et al.*, 2008].

[23] Figure 9 shows the time series of melt onset dates for every region, and for the entire Arctic, spanning 1979 to 2007. Large interannual variability in melt onset dates is evident, yet nearly all regions show a trend toward earlier melt over the last 28 years. It is noteworthy that the melt onset date for 2007 is not particularly early, and thus, earlier than normal melt onset does not appear to have contributed significantly toward the dramatic ice loss observed that year. Earlier formation of open water areas is important as it boosts the ice-albedo feedback back process, and thus contributes to enhanced melt in summer [e.g., *Perovich et al.*, 2008]. Although the melt onset was not unusual, subsequent autumn freezeup following the 2007 record minimum was striking (i.e., Figure 10). Freezeup dates for the central Arctic and the Chukchi/Beaufort seas were significantly later than normal (Figure 10). On average, freezeup in the central Arctic occurred about 20 days later in 2007 compared to 2006 (22 days for early freeze, 19 days for freeze) and 15 days later in the Chukchi/Beaufort Sea for both early freeze and freeze. Although the winter sea ice extent recovered from the 2007 minimum, the shortened

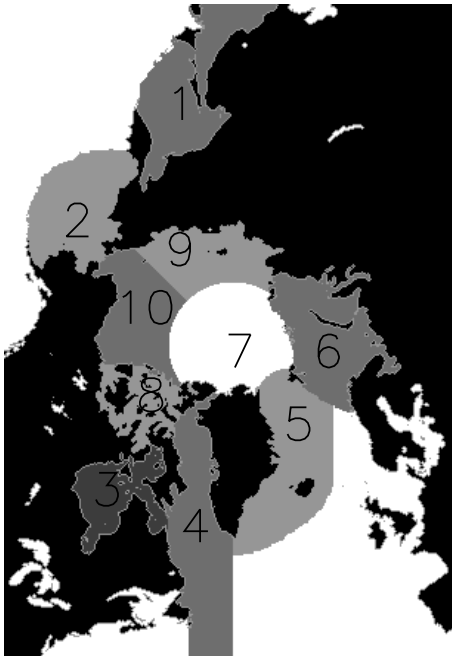

Figure 8. Illustration of different Arctic regions as used in Tables 2 and 3.

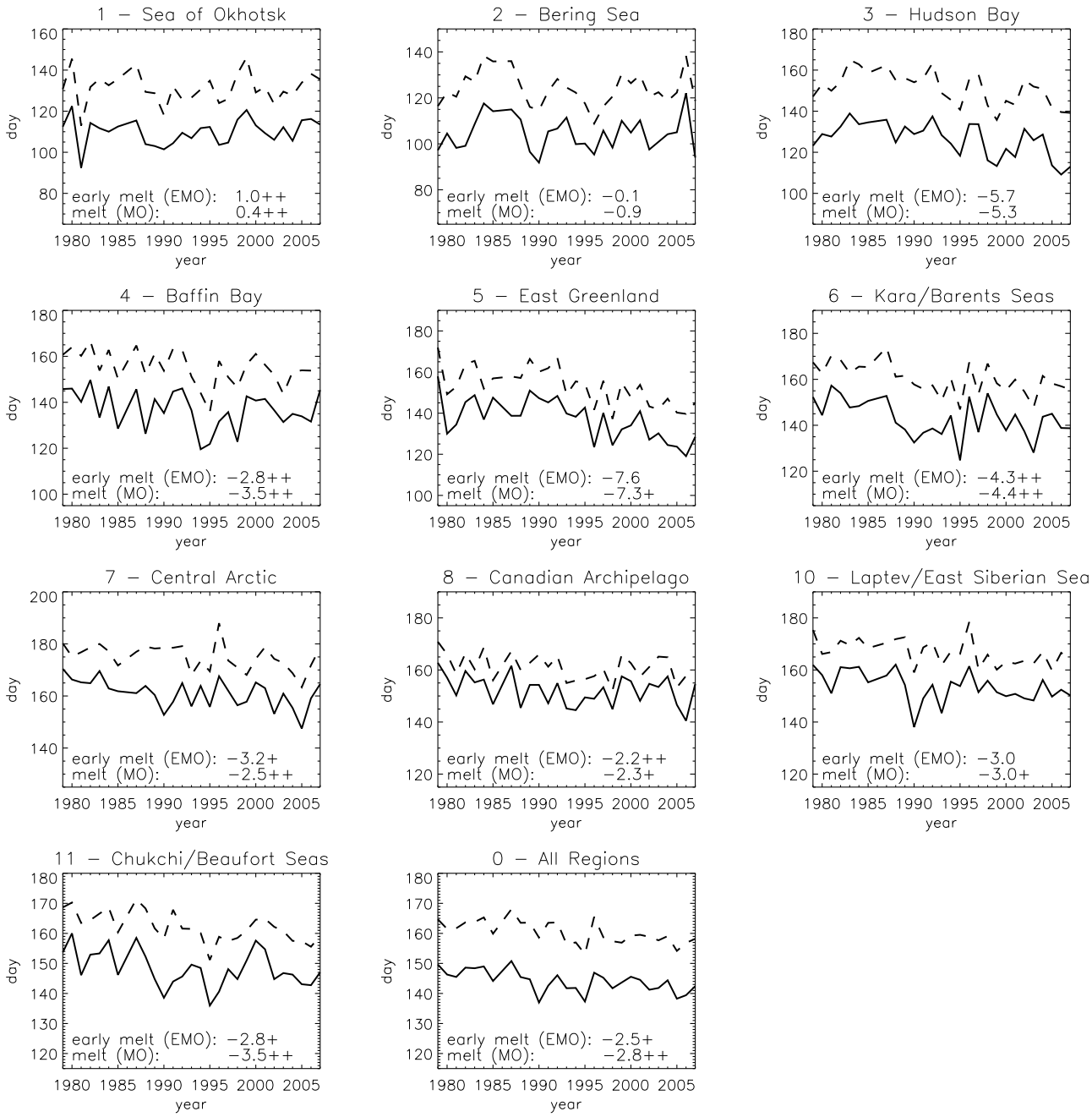

Figure 9. Melt onset days for the different regions (see also Figure 8). The solid lines indicate early melt (EMO); the dashed lines indicate melt (MO). The numbers show the trends in days decade^{-1}. Trends with plus sign are significant at the 95% confidence level, and trends with two plus signs are significant at the 99% confidence level.

length of the period of ice growth may in part explain the observed thin ice in 2008 derived from radar data in about the same region [*Giles et al.*, 2008].

[24] In general there is less interannual variability in the freezeup dates as freezeup is largely governed by cooling atmospheric temperatures as the sun sets. However, in the last several years, large expanses of open water have remained at the end of the summer melt period, in regions such as the Laptev/East Siberian seas, Chukchi/Beaufort seas and the central Arctic. Since time is needed for the ocean mixed layer to lose the heat gained during the summer, autumn freezeup is subsequently delayed. In general, trends in freezeup are larger than those for the melt onset. The melt season length for each year is plotted in Figure 11. With the exception of the Sea of Okhotsk and the Bering Sea all other regions show an obvious increase in melt season length.

[25] Table 3 quantifies trends in melt onset, freezeup, and melt length for the entire SMMR-SSM/I period for the entire Arctic for the different regions. Except for the Sea

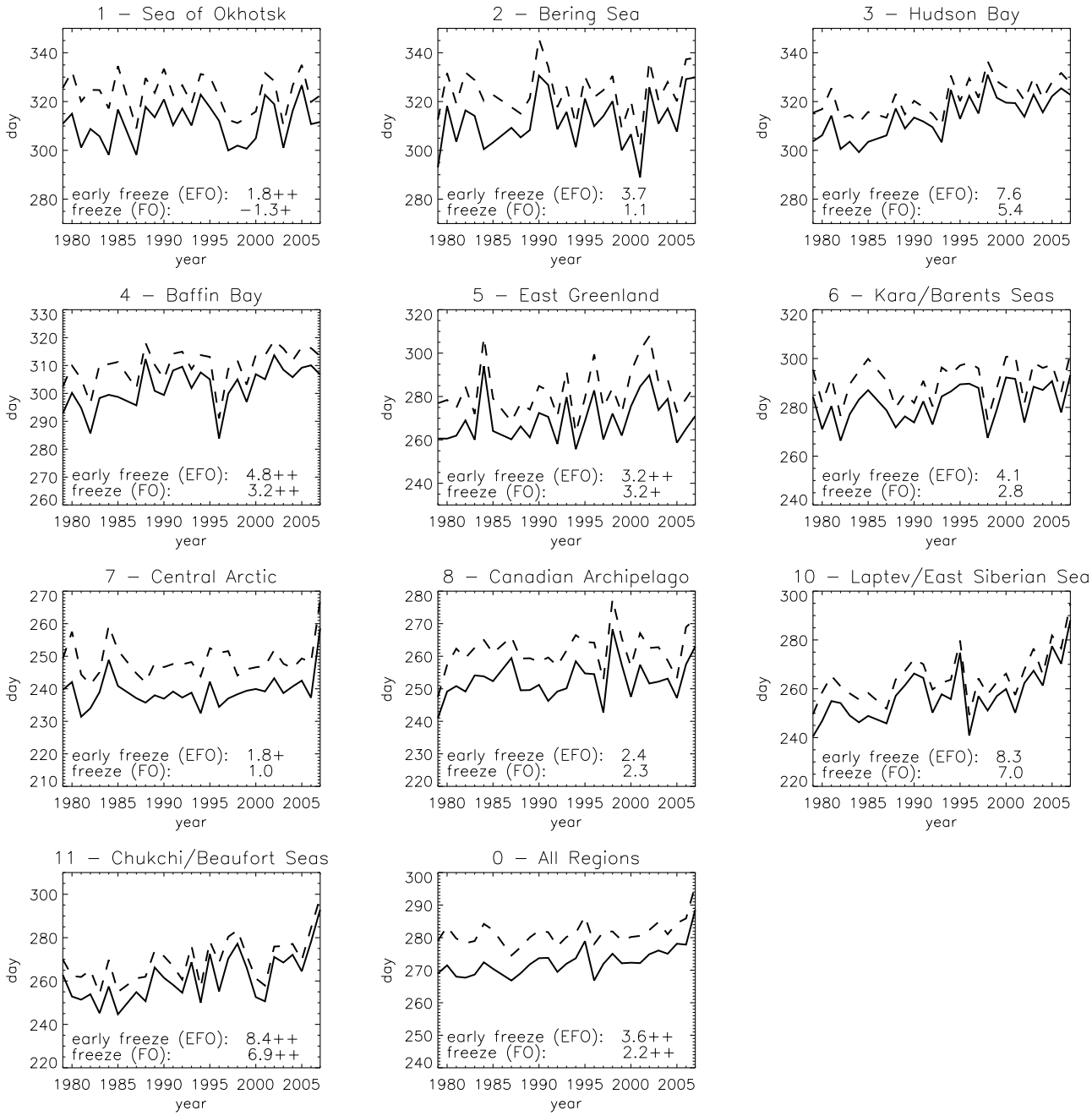

Figure 10. Freeze onset days for the different regions (see also Figure 8). The solid lines indicate early freeze (EFO) and the dashed line indicates freeze (FO). The numbers show the trends in days decade^{-1}. Trends with plus sign are significant at the 95% confidence level, and trends with two plus signs are significant at the 99% confidence level.

of Okhotsk and the Bering Sea, melt season length trends are statistically significant at the 95% confidence level. For the vast majority of the Arctic, melt onset is beginning earlier. The largest trend is observed for the East Greenland Sea with a trend of −7.6 d decade^{-1} for EMO and −7.3 d decade^{-1} for MO.

[26] The largest trends in freezeup are observed in the Laptev/East Siberian Seas and Chukchi/Beaufort Seas with trends between 6.9 and 8.4 d decade^{-1}. The Laptev/East Siberian Seas have the most significant and consistent delay in autumn freezeup, starting in 1996, compared to the other regions. The trend for the entire Arctic in melt season length is positive for both "inner" (EFO–MO) and "outer" (FO–EMO) melt length (6.4 d decade^{-1} and 4.7 d decade^{-1}, respectively). These trends are also similar to the trends observed by *Belchansky et al.* [2004] (5.5 d decade^{-1}) and *Smith* [1998b] (5.2 d decade^{-1} for the MY ice).

[27] It is also worth noting that in three of the four regions with the greatest trends in melt season length (Hudson Bay, Laptev/East Siberian seas, Chukchi/Beaufort seas) the trend

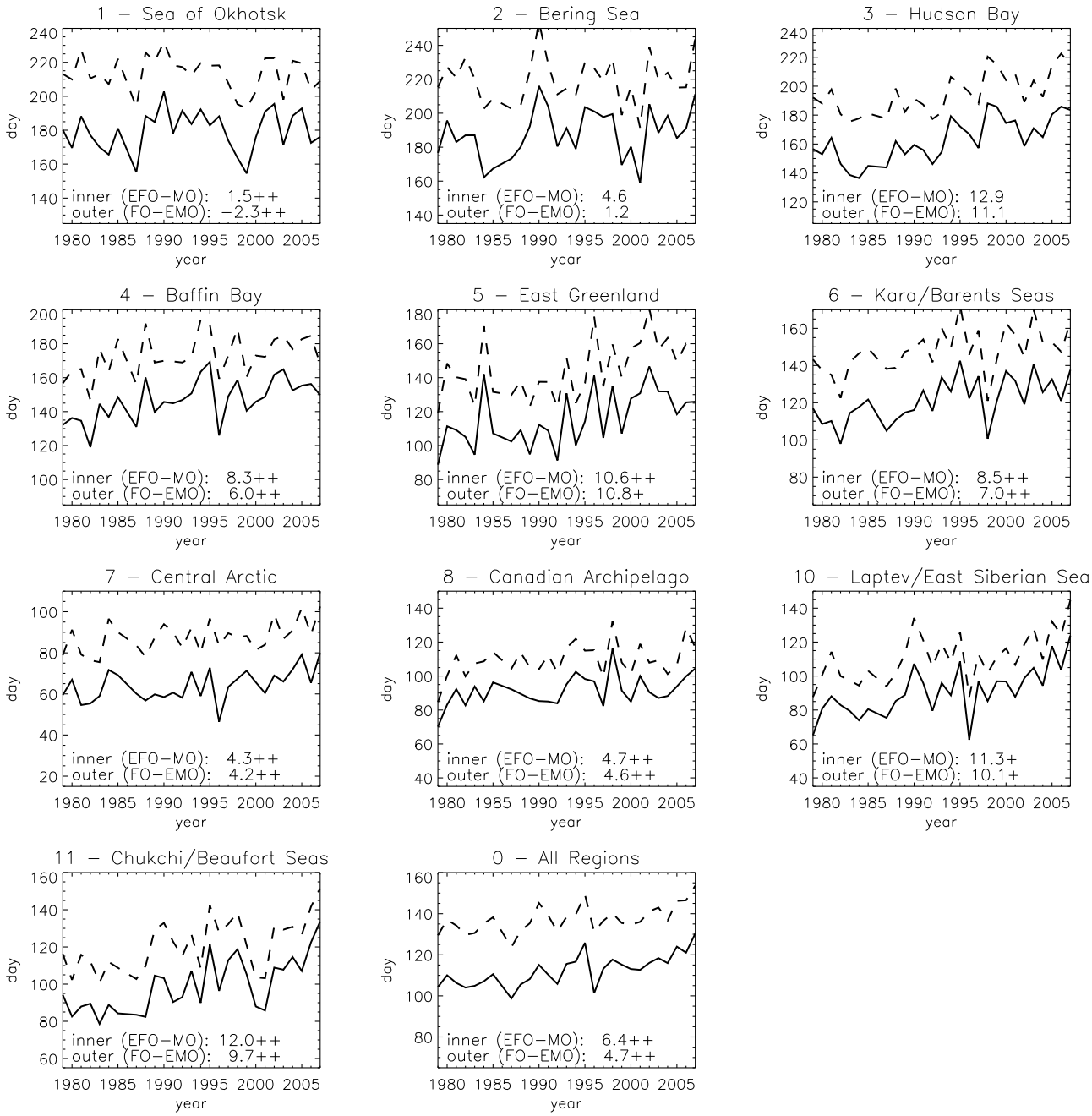

Figure 11. Melt season length for the different regions (see Figure 8) and the entire Arctic. The solid lines indicate the length of continuous melt (EFO–MO), and dashed lines indicates the length between the first day of melt until the last day of melt (FO–EMO). The numbers show the trends in days decade^{-1}. Trends with plus sign are significant at the 95% confidence level, and trends with two plus signs are significant at the 99% confidence level.

in freeze onset is about twice as large as the trend in melt onset. The reason is that with an earlier melt onset the mixed layer of the Arctic Ocean will have more time to warm up further delaying autumn freezeup.

5. Conclusion

[28] Melt and freeze onset dates are calculated for the entire Arctic using satellite passive microwave data. The algorithm also distinguishes between the first occurrence of melt and continuous summer melt. Similarly, the first onset of freeze and the day of continuous freeze are extracted.

[29] With the exception of the Sea of Okhotsk, all areas in the Arctic show a trend toward earlier melt onset and also a trend toward later freezeup. For the entire Arctic, the melt season has lengthened at a rate of 6.4 d decade^{-1} when only the period of continuous melt is considered, and 4.7 d decade^{-1} when the period between the first day of melt and the last day of melt is considered. Largest trends of over 10 d decade^{-1} are seen for Hudson Bay, the East Greenland

Table 3. Trends of Melt and Freeze Onset Days as Well as Trends in Melt Season Length for Different Regions[a]

Region	Early Melt (EMO)	Melt (MO)	Early Freeze (EFO)	Freeze (FO)	"Inner" Melt Length (EFO−MO)	"Outer" Melt Length (FO− EMO)
All	−2.5 ++	−2.8 ++	3.7 ++	2.2 +	6.4 ++	4.7 ++
Sea of Okhotsk (1)	1.0	0.4	1.8	−1.3	1.5	−2.3
Bering Sea (2)	−0.1	−1.0	3.7	1.1	4.6	1.2
Hudson Bay (3)	−5.7 ++	−5.3 ++	7.8 ++	5.4 ++	12.9 ++	10.1 ++
Baffin Bay (4)	−2.6	−3.4 +	4.6 ++	3.1 +	7.9 ++	5.6 +
East Greenland (5)	−7.6 ++	−7.3 ++	3.3	3.2	11.0 ++	10.8 ++
Kara/Barents seas (6)	−4.3 +	−4.4 ++	4.1 +	2.8	8.5 ++	7.1 ++
Central Arctic (7)	−3.2 ++	−2.5 +	1.8	1.0	4.3 ++	4.2 ++
Canadian Archipelago (8)	−2.2	−2.3 +	2.4	2.3	4.7 +	4.6 +
Laptev/East Siberian seas (9)	−3.0 +	−3.0 ++	8.3 ++	7.0 ++	11.3 ++	10.1 ++
Chukchi/Beaufort seas (10)	−2.8 +	−3.5 ++	8.4 ++	6.9 ++	12.0 ++	9.7 ++

[a]Units are in days decade^{-1}. Trends with "+" are significant at the 95% confidence level, and trends with "++" are significant at the 99% confidence level. See also Figure 8 for illustration of regions.

Sea, the Laptev/East Siberian Seas, and the Chukchi/Beaufort Seas. This means that from 1979 to 2007, the melt season has lengthened by almost 20 d.

[30] Today the thickness distribution in the Arctic is very different than it was in the 1980s. In spring 2008, 73% of the Arctic Basin consisted of thin, first-year ice, and the extremely old ice (i.e., older than 7 years) had essentially disappeared [e.g., *Maslanik et al.*, 2007]. Since the ice is thinner overall today than in the 1980s, and the melt is happening earlier and earlier, open water areas develop earlier than before, and become more extensive throughout the summer. These open water areas absorb solar radiation, heat up, and foster more melting of the ice [*Perovich et al.*, 2007, 2008]. This feedback process has always been present, yet with more extensive open water areas, this feedback process becomes even stronger and further boosts ice loss. The subsequent increased warming of the mixed layer of the Arctic Ocean results in a trend toward later freezeup, further reducing the sea ice mass. The later freeze onset also has ramifications on the eventual maximum sea ice cover the following winter. Additionally, marine ecosystems are very sensitive to changes in melt onset and freezeup dates. Thus accurate and consistent long-term records of melt onset and freezeup are needed to better understand changes and feedbacks of the Arctic sea ice cover. This algorithm provides the first comprehensive (1979 through present) record of both melt onset and freezeup for the Arctic.

[31] **Acknowledgments.** The authors like to thank the reviewers for their constructive comments and the colleagues who have been using the data set for their feedback.

References

Abdalati, W., K. Steffen, C. Otto, and K. C. Jezek (1995), Comparison of brightness temperatures from SSM/I instruments on the DMSP F8 and F11 satellites for Antarctica and the Greenland ice sheet, *Int. J. Remote Sens.*, *16*, 1223–1229, doi:10.1080/01431169508954473.

Belchansky, G. I., D. C. Douglas, and N. G. Platonov (2004), Duration of the Arctic sea ice melt season: Regional and interannual variability, 1979–2001, *J. Clim.*, *17*, 67–80, doi:10.1175/1520-0442(2004)017<0067:DOTASI>2.0.CO;2.

Colton, M. C., and G. A. Poe (1999), Intersensor calibration of DMSP SSM/I's: F-8 to F-14, 1987–1997, *IEEE Trans. Geosci. Remote Sens.*, *37*, 418–439, doi:10.1109/36.739079.

Drinkwater, M. R., and X. Liu (2000), Seasonal to interannual variability in Antarctic sea-ice surface melt, *IEEE Trans. Geosci. Remote Sens.*, *38*, 1827–1842, doi:10.1109/36.851767.

Drobot, S. D., and M. R. Anderson (2001), An improved method for determining snowmelt onset dates over Arctic sea ice using scanning multichannel microwave radiometer and Special Sensor Microwave/Imager data, *J. Geophys. Res.*, *106*, 24,033–24,049, doi:10.1029/2000JD000171.

Forster, R. R., D. G. Long, K. C. Jezek, S. D. Drobot, and M. R. Anderson (2001), The onset of Arctic sea-ice snowmelt as detected with passive- and active-microwave remote sensing, *Ann. Glaciol.*, *33*, 85–93, doi:10.3189/172756401781818428.

Giles, K. A., S. W. Laxon, and A. L. Ridout (2008), Circumpolar thinning of Arctic sea ice following the 2007 record ice extent minimum, *Geophys. Res. Lett.*, *35*, L22502, doi:10.1029/2008GL035710.

Gloersen, P., D. J. Cavalieri, W. J. Campbell, and H. J. Zwally (1990), *Nimbus-7 SMMR Polar Radiances and Arctic and Antarctic Sea Ice Concentrations*, [CD-ROM], Natl. Snow Ice Data Cent., Boulder, Colo.

Harouche, I. P. F., and D. G. Barber (2001), Seasonal characterization of microwave emissions from snow-covered first-year sea ice, *Hydrol. Process.*, *15*, 3571–3583, doi:10.1002/hyp.1034.

Howell, S. E. L., A. Tivy, J. J. Yackel, B. G. T. Else, and C. R. Duguay (2008), Changing sea ice melt parameters in the Canadian Arctic Archipelago: Implications for the future presence of multiyear ice, *J. Geophys. Res.*, *113*, C09030, doi:10.1029/2008JC004730.

Jezek, K. C., C. J. Merry, and D. J. Cavalieri (1993), Comparison of SMMR and SSM/I passive microwave data collected over Antarctica, *Ann. Glaciol.*, *17*, 131–136.

Kalnay, E., et al. (1996), The NCEP/NCAR 40-year reanalysis project, *Bull. Am. Meteorol. Soc.*, *77*, 437–470, doi:10.1175/1520-0477(1996)077<0437:TNYRP>2.0.CO;2.

Kwok, R., G. F. Cunningham, and S. V. Nghiem (2003), A study of melt onset in RADARSAT SAR imagery, *J. Geophys. Res.*, *108*(C11), 3363, doi:10.1029/2002JC001363.

Livingstone, C. E., K. P. Singh, and A. L. Gray (1987), Seasonal and regional variations of active/passive microwave signatures of sea ice, *IEEE Trans. Geosci. Remote Sens.*, *GE-25*, 159–173, doi:10.1109/TGRS.1987.289815.

Markus, T., and D. J. Cavalieri (1998), Snow depth distribution over sea ice in the Southern Ocean from satellite passive microwave data, in *Antarctic Sea Ice: Physical Processes, Interactions, and Variability*, *Antarct. Res. Ser.*, vol. 74, edited by M. O. Jeffries, pp. 19–40, AGU, Washington, D. C.

Maslanik, J., and J. C. Stroeve (1990), *DMSP SSM/I daily gridded brightness temperatures, 1987–2008*, Natl. Snow and Ice Data Cent., Boulder, Colo.

Maslanik, J. A., C. Fowler, J. Stroeve, S. Drobot, J. Zwally, D. Yi, and W. Emery (2007), A younger, thinner Arctic ice cover: Increased potential for rapid, extensive sea-ice loss, *Geophys. Res. Lett.*, *34*, L24501, doi:10.1029/2007GL032043.

Perovich, D. K., S. V. Nghiem, T. Markus, and A. Schweiger (2007), Seasonal evolution and interannual variability of the local solar energy absorbed by the Arctic sea ice–ocean system, *J. Geophys. Res.*, *112*, C03005, doi:10.1029/2006JC003558.

Perovich, D. K., J. A. Richter-Menge, K. F. Jones, and B. Light (2008), Sunlight, water, and ice: Extreme Arctic sea ice melt during the summer of 2007, *Geophys. Res. Lett.*, *35*, L11501, doi:10.1029/2008GL034007.

Rigor, I. G., R. L. Colony, and S. Martin (2000), Variations in surface air temperature observations in the Arctic, 1979–97, *J. Clim.*, *13*, 896–914, doi:10.1175/1520-0442(2000)013<0896:VISATO>2.0.CO;2.

Smith, D. M. (1998a), Observation of perennial Arctic sea ice melt and freeze-up using passive microwave data, *J. Geophys. Res.*, *103*, 27,753–27,769, doi:10.1029/98JC02416.

Smith, D. M. (1998b), Recent increase in the length of the melt season of perennial Arctic sea ice, *Geophys. Res. Lett.*, *25*, 655–658, doi:10.1029/98GL00251.

Stroeve, J., J. Maslanik, and L. Xiaoming (1998), An intercomparison of DMSP F11- and F13-derived sea ice products, *Remote Sens. Environ.*, *64*, 132–152, doi:10.1016/S0034-4257(97)00174-0.

Stroeve, J., M. Serreze, S. Drobot, S. Gearheard, M. Holland, J. Maslanik, W. Meier, and T. Scambos (2008), Arctic sea ice extent plummets in 2007, *Eos Trans. AGU*, *89*(2), doi:10.1029/2008EO020001.

Stroeve, J. C., M. C. Serreze, F. Fetterer, T. Arbetter, W. Meier, J. Maslanik, and K. Knowles (2005), Tracking the Arctic's shrinking ice cover: Another extreme September minimum in 2004, *Geophys. Res. Lett.*, *32*, L04501, doi:10.1029/2004GL021810.

Ulaby, F. T., R. K. Moore, and A. K. Fung (1986), *Microwave Remote Sensing: Active and Passive, From Theory to Applications*, Artech House, Norwood, Mass.

Winebrenner, D. P., E. D. Nelson, R. Colony, and R. D. West (1994), Observation of melt onset on multiyear Arctic sea ice using the ERS-1 synthetic aperture radar, *J. Geophys. Res.*, *99*, 22,425–22,441, doi:10.1029/94JC01268.

T. Markus, Cryospheric Sciences Branch, NASA Goddard Space Flight Center, Code 614.1, Greenbelt, MD 20771, USA. (thorsten.markus@nasa.gov)

J. Miller, Wyle Information Sciences, NASA Goddard Space Flight Center, Greenbelt, MD 20771, USA.

J. C. Stroeve, National Snow and Ice Data Center, University of Colorado, Boulder, CO 80309, USA.